Biomech Model Mechanobiol (2016) 15:1713–1731
DOI 10.1007/s10237-016-0793-2

ORIGINAL PAPER

Development of a computational model for macroscopic predictions of device-induced thrombosis

Joshua O. Taylor[1,2] · **Richard S. Meyer**[2] · **Steven Deutsch**[2] · **Keefe B. Manning**[1,3]

Received: 14 July 2015 / Accepted: 27 April 2016 / Published online: 12 May 2016

Abstract While cardiovascular device-induced thrombosis is associated with negative patient outcomes, the convoluted nature of the processes resulting in a thrombus makes the full thrombotic network too computationally expensive to simulate in the complex geometries and flow fields associated with devices. A macroscopic, continuum computational model is developed based on a simplified network, which includes terms for platelet activation (chemical and mechanical) and thrombus deposition and growth in regions of low wall shear stress (WSS). Laminar simulations are performed in a two-dimensional asymmetric sudden expansion geometry and compared with in vitro thrombus size data collected using whole bovine blood. Additionally, the predictive power of the model is tested in a flow cell containing a series of symmetric sudden expansions and contractions. Thrombi form in the low WSS area downstream of the asymmetric expansion and grow into the nearby recirculation region, and thrombus height and length largely remain within 95 % confidence intervals calculated from the in vitro data for 30 min of blood flow. After 30 min, predicted thrombus height and length are 0.94 and 4.32 (normalized by the 2.5 mm step height). Importantly, the model also correctly predicts locations of thrombus deposition observed in the in vitro flow cell of expansions and contractions. As the simulation results, which rely on a greatly reduced model of the thrombotic network, are still able to capture the macroscopic behavior of the full network, the model shows promise for timely predictions of device-induced thrombosis toward optimizing and expediting the device development process.

Keywords Device-induced thrombosis · Wall shear stress · Platelet activation · Computational fluid dynamics · Thrombus growth · Flow separation

✉ Keefe B. Manning
kbm10@psu.edu

[1] Department of Biomedical Engineering, The Pennsylvania State University, 205 Hallowell Building, University Park, PA 16802, USA

[2] Applied Research Laboratory, The Pennsylvania State University, State College, PA, USA

[3] Department of Surgery, Penn State Hershey Medical Center, Hershey, PA, USA

List of symbols

$\boldsymbol{u}$	Velocity
p	Pressure
t	Time
ν	Kinematic viscosity
ρ	Density
F	Modified Brinkman function
ε	Aggregation intensity
ε_{t}	Aggregation intensity threshold
k	Thrombus permeability
Q	Arbitrary scalar quantity
D	Diffusivity
R	Sources and sinks
ϕ_{n}	Non-activated platelet concentration
ϕ_{a}	Activated platelet concentration
D_{n}	Diffusion coefficient for non-activated platelets
D_{a}	Diffusion coefficient for activated platelets
A_{C}	Chemical platelet activation rate
ADP	Adenosine diphosphate (ADP) concentration
$\mathrm{ADP}_{\mathrm{t}}$	ADP threshold for chemical activation
t_{ADP}	Characteristic time for chemical activation

A_{M}	Mechanical platelet activation rate
τ	Scalar shear stress
$\bar{\bar{\boldsymbol{\sigma}}}$	Viscous stress tensor
ϕ_{f}	Activated platelet fraction
C	Power law coefficient
α	Power law coefficient
β	Power law coefficient
D_{ADP}	Diffusion coefficient for ADP
R_{ADP}	Amount of ADP in a platelet
α_{ε}	Thrombus volumetric growth rate
τ_{w}	Wall shear stress (WSS)
P_{TSP}	Weighting function for thrombus deposition /growth
$\tau_{\mathrm{low,wall}}$	Low WSS threshold for thrombus deposition
$\tau_{\mathrm{high,wall}}$	High WSS threshold for thrombus deposition
$\tau_{\mathrm{low,thrombus}}$	Low WSS threshold for thrombus growth
$\tau_{\mathrm{high,thrombus}}$	High WSS threshold for thrombus growth
β_{ε}	Thrombus breakdown function
B	Thrombus breakdown rate
$\tau_{\mathrm{breakdown,wall}}$	WSS threshold for thrombus breakdown at a wall
$\tau_{\mathrm{breakdown,thrombus}}$	WSS threshold for thrombus breakdown at a thrombus surface
U	Average inlet velocity
h	Step height
$\phi_{\mathrm{a},i}$	Initial (background) concentration of activated platelets
$\phi_{\mathrm{n},i}$	Initial concentration of non-activated platelets
t_{G}	Characteristic thrombus growth time
H	Thrombus height
L	Thrombus length

1 Introduction

Clinicians are increasingly using blood-contacting devices for the treatment of a variety of cardiovascular conditions; unfortunately, thrombosis remains an issue. Thrombosis is a complex phenomenon but has long been understood to depend primarily on the interactions of the three components of Virchow's triad: blood constituents, blood flow, and surface properties. Platelets, enzymes, and 13 chemical factors are among the species involved in the thrombotic process, and there are at least 80 coupled reactions that regulate thrombus growth (Cito 2013). The thrombotic process also occurs on multiple spatial and temporal scales. The spatial scales range from angstroms (e.g., calcium ions) to micrometers (e.g., platelets) to millimeters and centimeters (e.g., vessel diameters). The timescales range from microseconds (e.g., intracellular processes) to milliseconds (e.g., platelet adhesion) to minutes and hours (e.g., macroscopic thrombus growth). The complexity of the thrombotic process, combined with its multi-scale nature, makes modeling thrombosis an arduous task.

In spite of this, many thrombosis and blood coagulation models are available in the literature (Xu et al. 2011; Wang and King 2012; Cito 2013; Leiderman and Fogelson 2014). These are either single-scale [focusing on a single spatial scale; e.g., (Fogelson 1992; Sorensen et al. 1999a; Goodman et al. 2005)] or multi-scale [(coupling processes on multiple spatial scales; e.g., (Xu et al. 2008, 2009, 2010; Leiderman and Fogelson 2011)]. The majority of these focus on hemostasis or vascular thrombosis, using an "injury zone" or similar boundary condition to initiate aggregation. This approach is appropriate for modeling thrombosis or coagulation in response to vessel injury or plaque rupture; however, the lack of precise a priori knowledge of thrombosis sites in devices renders this approach ineffective for predictions of device-induced thrombosis. Also, while multi-scale models present a more accurate representation of the microscopic aspects of the thrombotic process, they are generally more computationally expensive when compared to single-scale models. Consequently, using multi-scale models to simulate thrombosis in the geometries associated with blood-contacting devices can lead to prohibitively long simulation times.

Fogelson (1992) first proposed the framework for a computational model of platelet activation and aggregation on a continuum. The model considers platelets (non-activated and activated) and a lumped platelet agonist concentration and couples an aggregate to the velocity field using a cohesive stress body force that acts as a momentum sink in the Navier–Stokes equations. Fogelson and Guy (2008) extended the initial continuum model by considering platelet–platelet cohesion separately from platelet-wall adhesion. They compared a multi-scale model (one scale on the order of platelets and the other on the scale of the diameter of a large blood vessel) of platelet thrombosis to a single-scale (only on the scale of a large blood vessel) reduction of the multi-scale model, achieving reasonable agreement in simple test cases. Importantly, they showed their single-scale model produced similar macroscopic results to their multi-scale model in only about 1 % of the computational time (Fogelson and Guy 2008).

Goodman et al. (2005) attempted to simulate device-induced thrombosis using a single-scale model, which was capable of providing predictions of platelet adhesion, thrombus growth, and embolization. To focus on low-flow devices, such as hemodialyzers or oxygenators, only agonist-induced platelet activation was considered in the bulk flow, but adhered platelets could be activated by shear stress. Their model contains source terms for platelet adhesion at material and thrombus surfaces, which are independent of the local wall shear stress (WSS), and coupled a growing thrombus to

the velocity field by increasing the fluid viscosity 100,000-fold in cells that are considered to be "thrombus." They were able to validate initial locations of platelet adhesion and relative rates of thrombus embolization with experimental data. Another attempt at simulating device-induced thrombosis was made by Tamagawa et al. (2009). They used the Lattice–Boltzmann method to predict locations of thrombus deposition in an asymmetric sudden expansion. They visually validated their simulations with in vitro data that showed thrombus deposition at the expansion and reattachment point.

While most thrombosis models have been at least partially validated with in vitro or in vivo data, one aspect of macroscopic thrombosis models has remained difficult to validate: thrombus growth. The primary reason for this is the lack of macroscopic thrombus growth data for comparison with simulations. However, Taylor et al. (2014) conducted a recent in vitro study of time-dependent thrombus size, in which they used magnetic resonance imaging (MRI) to quantify thrombus size over increasing durations of whole bovine blood circulation through an asymmetric sudden expansion. The expansion caused flow separation, producing a region of low WSS that is relevant to blood-contacting devices. Additionally, they used the three-dimensional topographies of the thrombi to create computational meshes for use in computational fluid dynamics (CFD) simulations to calculate the thrombus surface shear stresses. Both the in vitro thrombus growth data and the in silico thrombus surface shear stress data can be used in the development and validation of thrombosis models.

For the purpose of medical device development, a macroscopic thrombosis model, capable of predicting locations of thrombus deposition and subsequent growth under conditions relevant to device-induced thrombosis, is needed. Unfortunately, none of the existing models have been used to predict thrombosis in three dimensions on the spatial and temporal scales relevant to medical devices. While there are many events occurring at microscopic scales in the thrombotic process, only a continuum approach on a macroscopic scale will allow for thrombus size predictions on temporal and spatial scales relevant to most blood-contacting devices. To accomplish this, the convoluted network that regulates thrombosis must be reduced to a smaller and more streamlined network that relies primarily on fluid mechanics to predict thrombus deposition and growth, while maintaining the macroscopic behavior of the full network. A computational model to predict device-induced thrombosis must (1) consider chemical and mechanical platelet activation, (2) use the fluid mechanics of the system to determine locations of thrombus deposition and the rate of thrombus growth, (3) allow for the coupling of the fluid velocity field to a growing thrombus, and (4) provide verifiable predictions of thrombus size on a spatial scale that is the same order of magnitude as the device and on a temporal scale of minutes to hours. A thrombosis model capable of satisfying all four of these requirements is presented here.

2 Materials and methods

2.1 Model governing equations

A continuum model for platelet aggregation proposed by Fogelson (1992) is modified to predict device-induced thrombosis. Fogelson's model considers bulk concentrations of three species: non-activated platelets, activated platelets, and a chemical activator. In addition, the concentrations of platelet–platelet links and a cohesive stress tensor are tracked to quantify aggregation and couple it to the velocity field. Fogelson's model relies on boundary conditions to dictate locations of platelet adhesion and aggregation and does not account for mechanical activation of platelets.

To convert Fogelson's (1992) model to work with device-induced thrombosis, some major modifications are made. Terms are added to predict thrombus deposition in regions of low WSS and the degradation of thrombus in regions of high WSS. A diffusion term is added to the transport equation for activated platelets to allow them to move throughout the computational domain, especially in low-flow regions, along with a term to quantify mechanical platelet activation. The cohesive stress tensor is completely removed from the model, and a modified Brinkman term, used to simulate flow through porous media, is added to the Navier–Stokes equations to couple a growing thrombus to the velocity field. Finally, the platelet–platelet link variable is replaced with a variable representing thrombus aggregation intensity.

A network representation of the presented thrombosis model, illustrating the considered species, external stimuli, and interactions, is displayed in Fig. 1.

2.1.1 Fluid

The model assumes laminar flow of a Newtonian fluid, and the continuity equation (1) and the Navier–Stokes equations (2) are used to calculate the velocity ($\boldsymbol{u}$) and pressure (p) fields. A modified Brinkman term, resembling the Brinkman term used in a blood coagulation model proposed by Leiderman and Fogelson (2011), is added to the right-hand side of Eq. (2) to couple the growing thrombus and the velocity field. It depends on the fluid kinematic viscosity (ν), a function (F) based on the local aggregation intensity (ε), and the fluid velocity. F is calculated using Eq. (3) and depends on the thrombus permeability (k) and a threshold value of aggregation intensity necessary for a computational cell to be considered part of a thrombus (ε_t). The Brinkman term in Eq. (2) impedes fluid flow in regions of high aggregation

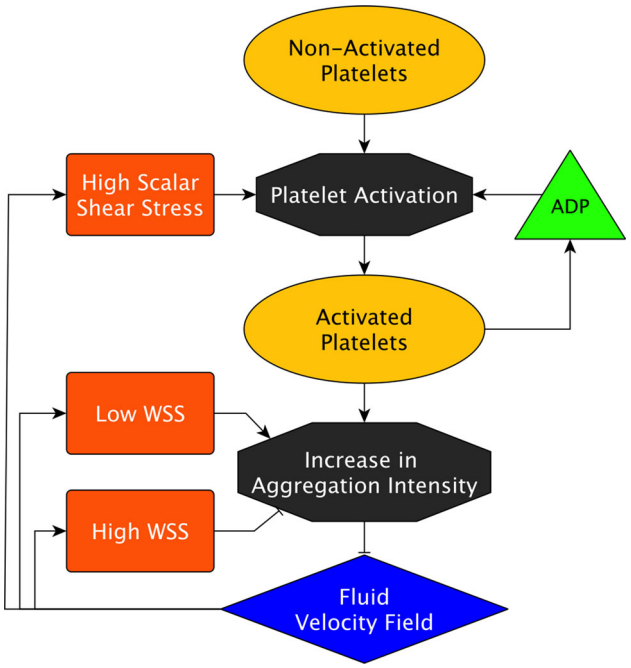

Fig. 1 A simple network representation of the presented thrombosis model. Cellular species are represented with *yellow ovals*, chemical species with *green triangles*, events with *gray octagons*, mechanical stimuli with *orange squares*, and vector fields with *blue diamonds*. Positive interactions are shown with *arrows*, while negative interactions are shown with *blunted lines*

intensity, ensures a thrombus is modeled as a porous material, provides a sharp boundary between the thrombus and fluid based on a threshold aggregation intensity, and allows the Navier–Stokes equations to be used throughout the entire computational domain without the need for fluid–structure interaction modeling.

$$\nabla \cdot \boldsymbol{u} = 0 \tag{1}$$

$$\frac{\partial \boldsymbol{u}}{\partial t} + (\boldsymbol{u} \cdot \nabla)\,\boldsymbol{u} = -\frac{1}{\rho}\nabla p + \nu \nabla^2 \boldsymbol{u} - \nu F(\varepsilon)\,\boldsymbol{u} \tag{2}$$

$$F(\varepsilon) = \begin{cases} 0 & \text{if } \varepsilon < \varepsilon_\mathrm{t} \\ \frac{1}{k}\frac{\varepsilon/\varepsilon_\mathrm{t}}{\varepsilon/\varepsilon_\mathrm{t}+1} & \text{if } \varepsilon \geq \varepsilon_\mathrm{t} \end{cases} \tag{3}$$

Equation (3) is nonzero only in areas where $\varepsilon \geq \varepsilon_\mathrm{t}$. Once this criterion is met, F increases nonlinearly with increasing ε. F is equal to half of its maximum value $(1/2k)$ when $\varepsilon = \varepsilon_\mathrm{t}$ and reaches 80 % of its maximum value when $\varepsilon = 4\varepsilon_\mathrm{t}$ (Fig. 2). As the continuous thrombus boundary is simulated in a discrete domain, the boundary will always intersect computational cells. F is formulated to provide approximately half the maximum flow restriction in cells on the thrombus surface (having an aggregation intensity just above the threshold) in an attempt to more accurately capture the fluid dynamics near a growing thrombus (i.e., in cells that would be intersected by the thrombus boundary in a continuum); however, as the

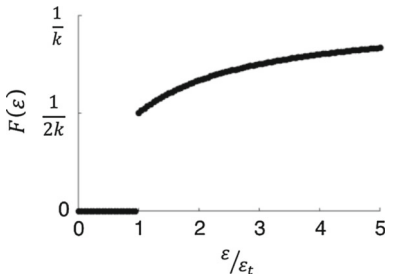

Fig. 2 Plot of the modified Brinkman function, Eq. (3), with the normalized aggregation intensity. F is zero when $\varepsilon/\varepsilon_\mathrm{t} < 1$ and is equal to $1/2k$ when $\varepsilon/\varepsilon_\mathrm{t} = 1$. F approaches $1/k$ as $\varepsilon/\varepsilon_\mathrm{t} \to \infty$

aggregation intensity is several times the aggregation intensity threshold within the thrombus, flow restriction in interior cells is closer to the maximum flow restriction, which mimics the internal thrombus architecture (Welsh et al. 2014). Additionally, k is small enough to ensure there is a substantial decrease in velocity within a simulated thrombus (i.e., there is no "blurring" of a simulated thrombus surface), even with only half of the maximum flow restriction applied in a thrombus boundary cell.

2.1.2 Model species

The thrombosis model does not track individual cells and particles, as their sizes are orders of magnitude smaller than the scale of the thrombosis model. Instead, bulk concentrations of three species are calculated in each computational cell: non-activated platelets, activated platelets, and adenosine diphosphate, ADP (a chemical activator). Platelets are the primary cellular mediator of thrombosis and normally exist in a non-activated, or quiescent, state. Platelet agonists or high shear stress can activate them either chemically or mechanically, respectively. Platelet agonists, including ADP, thromboxane A_2, and thrombin, also participate in feedback loops that continue to activate platelets even if the initial activating stimulus is removed. The proposed model focuses on ADP, which has been shown to be the primary chemical activator of platelets (Fogelson and Guy 2008). The species concentrations are calculated using convection–diffusion equations of the form shown in Eq. (4), where Q is an arbitrary scalar quantity, D is the diffusivity of Q, and R includes all sources and sinks of Q.

$$\frac{\partial Q}{\partial t} + (\boldsymbol{u} \cdot \nabla)\,Q = D\nabla^2 Q + R \tag{4}$$

2.1.3 Platelets

The concentrations of non-activated, ϕ_n, and activated, ϕ_a, platelets are calculated using Eqs. (5) and (6), respectively. Their respective diffusion coefficients, D_n and D_a, are

defined to be two orders of magnitude higher than expected for normal Brownian motion to account for an enhanced diffusivity due to the presence of red blood cells (RBCs) (Goldsmith and Turitto 1986), which do not explicitly appear in the model. Terms that are equal in magnitude but opposite in sign $\{[A_C\,(\mathrm{ADP})]\,\phi_n + [A_M\,(\phi_f, \tau)]\,(\phi_a + \phi_n)\}$ quantify the total rate of platelet activation (a sink for non-activated platelets and a source for activated platelets), based on chemical (A_C) and mechanical (A_M) stimuli. This ensures that mass is conserved in the platelet population.

$$\frac{\partial \phi_n}{\partial t} + (\boldsymbol{u} \cdot \nabla)\,\phi_n = D_n \nabla^2 \phi_n - \{[A_C\,(\mathrm{ADP})]\,\phi_n + [A_M\,(\phi_f, \tau)]\,(\phi_a + \phi_n)\} \quad (5)$$

$$\frac{\partial \phi_a}{\partial t} + (\boldsymbol{u} \cdot \nabla)\,\phi_a = D_a \nabla^2 \phi_a + \{[A_C\,(\mathrm{ADP})]\,\phi_n + [A_M\,(\phi_f, \tau)]\,(\phi_a + \phi_n)\} \quad (6)$$

Chemical platelet activation is quantified using a function of ADP concentration $[A_C\,(\mathrm{ADP})]$. This term is a linear rate equation with an activation threshold and is identical to one used by Sorensen et al. (1999a) for platelet activation by ADP. Consequently, a threshold concentration of ADP ($\mathrm{ADP_t}$) must be reached before any chemical activation of platelets occurs. The rate of chemical platelet activation also depends on a characteristic time, t_{ADP}.

$$A_C\,(\mathrm{ADP}) = \begin{cases} 0 & \text{for } \frac{\mathrm{ADP}}{\mathrm{ADP_t}} < 1 \\ \frac{\mathrm{ADP}}{(\mathrm{ADP_t})(t_{\mathrm{ADP}})} & \text{for } \frac{\mathrm{ADP}}{\mathrm{ADP_t}} \geq 1 \end{cases} \quad (7)$$

Mechanical platelet activation, a function of both shear stress and exposure time, is not accounted for in Fogelson's (1992) model. In the current model, mechanical activation $[A_M\,(\phi_f, \tau)]$ is quantified with a simplified form of a Lagrangian power law model proposed by Soares et al. (2013) that calculates increases in the platelet activation state (PAS) through stress history, scalar shear stress, and the stress rate. The PAS quantifies the level of platelet activation, between 0 and 1, and is assumed to be equivalent to the fraction of activated platelets (ϕ_f) for the present work: $\mathrm{PAS} = \phi_f = \phi_a/(\phi_a + \phi_n)$. If the terms accounting for stress history and stress rate are neglected, the power law can be used in an Eulerian model, and it reduces to Eq. (8), where C, α, and β are empirically determined coefficients that can be estimated from in vitro or in vivo data and τ is the scalar shear stress. The scalar shear stress, which gives a measure of the total shear stress acting on a fluid element based on the viscous stress tensor ($\bar{\bar{\boldsymbol{\sigma}}}$), is calculated following the procedure of Bludszuweit (1994) in Eq. (9) for use in Eq. (8). A reduced form of the Soares et al. (2013) model is also used in a platelet activation study by Hansen et al. (2015), in which Lagrangian and Eulerian mechanical platelet activation models are compared in an abdominal aortic aneurysm. Importantly, Hansen et al. (2015) found that predicted platelet activation only differed by ~1 % between the two classes of models, and in general, this is small compared to estimated background platelet activation levels, which can be up to 20 % (Kennedy et al. 1997).

$$A_M\,(\phi_f, \tau) = (1 - \phi_f)\, C^{\frac{1}{\beta}} \beta \phi_f^{\frac{\beta-1}{\beta}} \tau^{\frac{\alpha}{\beta}} \quad (8)$$

$$\tau = \frac{1}{\sqrt{3}} \sqrt{\begin{array}{l} \sigma_{xx}^2 + \sigma_{yy}^2 + \sigma_{zz}^2 - \sigma_{xx}\sigma_{yy} - \\ \sigma_{xx}\sigma_{zz} - \sigma_{yy}\sigma_{zz} + 3\left(\sigma_{xy}^2 + \sigma_{xz}^2 + \sigma_{yz}^2\right) \end{array}} \quad (9)$$

2.1.4 Adenosine diphosphate

The concentration of ADP is tracked using Eq. (10), which is similar to the chemical activator transport equation in Fogelson's (1992) model. The difference is that the rate of platelet activation includes mechanical stimuli. Similar to the equations for platelets, Eq. (10) contains terms to account for temporal and spatial (advection and diffusion) changes in ADP concentration. However, unlike the diffusion coefficients for platelets, the diffusion coefficient for ADP (D_{ADP}) is not increased above the normal value for Brownian motion, as ADP molecules are orders of magnitude smaller than RBCs. The only production term for ADP is due to the release of ADP by activated platelets, $R_{\mathrm{ADP}}\,\{[A_C\,(\mathrm{ADP})]\,\phi_n + [A_M\,(\phi_f, \tau)]\,(\phi_a + \phi_n)\}$, and this term preserves one of the primary feedback loops in the thrombotic process. Platelets store ADP in granules and release it upon activation, with the rate of ADP release calculated by multiplying the amount of ADP contained in a platelet (R_{ADP}) by the rate of platelet activation $\{[A_C\,(\mathrm{ADP})]\,\phi_n + [A_M\,(\phi_f, \tau)]\,(\phi_a + \phi_n)\}$.

$$\frac{\partial \mathrm{ADP}}{\partial t} + (\boldsymbol{u} \cdot \nabla)\,\mathrm{ADP} = D_{\mathrm{ADP}} \nabla^2 \mathrm{ADP} + R_{\mathrm{ADP}}\,\{[A_C\,(\mathrm{ADP})]\,\phi_n + [A_M\,(\phi_f, \tau)]\,(\phi_a + \phi_n)\} \quad (10)$$

2.1.5 Aggregation intensity

While Fogelson (1992) considered platelet–platelet links in his model to help quantify aggregation, the treatment of aggregation, or thrombus formation/growth, in the current model is significantly altered in several key ways: (1) Links between platelets are no longer explicitly considered, with a bulk variable quantifying the 'aggregation intensity' (ε) used instead, (2) the local aggregation intensity is used to couple the velocity field to a growing thrombus through Eq. (3), (3) neither advection nor diffusion of a thrombus is allowed (all thrombi are assumed to be anchored to a boundary), and (4) terms are included in Eq. (11) to account for thrombus deposition in regions of low WSS $[\alpha_\varepsilon P_{\mathrm{TSP}}\,(\tau_w)\,\phi_a^2]$ and thrombus breakdown in regions of high WSS $[\beta_\varepsilon\,(\tau_w)\,\varepsilon]$, which are

quantified by increases and decreases in ε, respectively. The idea of using an aggregation intensity parameter to quantify the extent of thrombus deposition and growth is based on work by Fogelson and Guy (2008). The aggregation intensity can loosely be thought of as a measure of thrombus density; however, the aggregation intensity is unbounded and has no true physical parallel. Nevertheless, the impact of the aggregation intensity on physical variables, such as the fluid velocity and pressure, is bounded through the modified Brinkman term (see Fig. 2).

$$\frac{\partial \varepsilon}{\partial t} = \alpha_\varepsilon P_{\mathrm{TSP}}(\tau_{\mathrm{w}})\,\phi_{\mathrm{a}}^2 - \beta_\varepsilon(\tau_{\mathrm{w}})\,\varepsilon \tag{11}$$

The novel term for thrombus deposition and growth in regions of low WSS involves a constant that controls the volumetric rate of thrombus formation and growth (α_ε), a weighting function based on the local WSS [$P_{\mathrm{TSP}}(\tau_{\mathrm{w}})$], and the square of the local concentration of activated platelets. Aggregation is defined to be proportional to the square of activated platelets, and this quadratic relationship has been observed in vitro (Gear 1982). The weighting function, Eq. (12), is based on a thrombus susceptibility potential (TSP) developed by Medvitz (2008), which has successfully been used to quantify the risk of thrombosis in blood-contacting devices (Topper et al. 2014). The TSP provides the instantaneous probability of thrombus deposition. Equation (12) relies on material-dependent high and low WSS thresholds (τ_{high} and τ_{low}, respectively) to control thrombus deposition (increases in aggregation intensity adjacent to a domain boundary) and growth (increases in aggregation intensity adjacent to the surface of a formed thrombus). The WSS (τ_{w}) for thrombus deposition to a solid surface is calculated by multiplying the fluid dynamic viscosity by the surface normal velocity gradient, while τ_{w} for thrombus growth is calculated by multiplying the fluid dynamic viscosity by the magnitude of a Jacobian matrix (the gradient of the local velocity field). Similarly, these two definitions of τ_{w} are used to estimate the breakdown of a thrombus in regions of high WSS using the local aggregation intensity and a weighting function based on the local WSS [$\beta_\varepsilon(\tau_{\mathrm{w}})$]. The weighting function, displayed as Eq. (13), uses a threshold WSS value for thrombus breakdown ($\tau_{\mathrm{breakdown}}$) and a constant defining the breakdown rate (B).

$$P_{\mathrm{TSP}}(\tau_{\mathrm{w}}) = \begin{cases} 1 & \text{for } |\tau_{\mathrm{w}}| \le \tau_{\mathrm{low}} \\ 1 - \frac{|\tau_w|}{\tau_{\mathrm{high}}} \cdot \frac{e^{\frac{|\tau_{\mathrm{w}}|-\tau_{\mathrm{low}}}{\tau_{\mathrm{high}}-\tau_{\mathrm{low}}}}-1}{e^1-1} & \text{for } \tau_{\mathrm{low}} < |\tau_{\mathrm{w}}| < \tau_{\mathrm{high}} \\ 0 & \text{for } |\tau_{\mathrm{w}}| \ge \tau_{\mathrm{high}} \end{cases} \tag{12}$$

$$\beta_\varepsilon(\tau_{\mathrm{w}}) = \begin{cases} 0 & \text{for } |\tau_{\mathrm{w}}| < \tau_{\mathrm{breakdown}} \\ B & \text{for } |\tau_{\mathrm{w}}| \ge \tau_{\mathrm{breakdown}} \end{cases} \tag{13}$$

For thrombus deposition, Eq. (12) is only evaluated in computational cells that have at least one face on a computational domain wall; for thrombus growth, Eq. (12) is only evaluated in cells contained within or at the surface of a thrombus. As the surface of a growing thrombus is not explicitly tracked in the model, the aggregation intensity threshold used in Eq. (9) establishes which cells are considered to be within a thrombus. If a cell satisfies the condition $\varepsilon \ge \varepsilon_{\mathrm{t}}$, it is considered to be within a thrombus, and all of its neighboring cells (those that share a face with the initial cell) with $\varepsilon < \varepsilon_{\mathrm{t}}$ are considered to be on the surface of the thrombus. Those cells are eligible for thrombus deposition based on Eq. (12) and a rate scaled by the inverse of the distance between the cell centers.

2.1.6 Determination of model parameters

The thrombosis model requires values for 18 parameters before it can be used to predict thrombus growth. When possible, parameter values are taken from the literature; however, some are estimated from time-dependent, in vitro thrombus size data (Taylor et al. 2014)—see Sect. 2.2 for details of the in vitro experiments. All parameters used in the thrombosis model, their values, and their sources are listed in Table 1.

One parameter calculated using in vitro data is α_ε, the coefficient dictating the volumetric rate of thrombus growth in Eq. (11). Taylor et al. (2014) observed that asymptotic thrombus size occurred after 45 min of blood circulation, at which point thrombus volume had reached approximately 0.1 cm^3. They also observed roughly linear growth until the asymptotic volume was reached, with a slope of 3.7×10^{-5} cm^3/s. This value is used for α_ε. Additionally, they used CFD to estimate the surface shear stresses on thrombi of different sizes and determined that mean values were generally between 0.5 and 0.75 $\mathrm{dyn/cm}^2$, regardless of thrombus size. Using these results, the high WSS thresholds for thrombus deposition and growth are taken to be 1.5 (double the highest mean value) and 3 $\mathrm{dyn/cm}^2$ (four times the highest mean value), respectively. Prior experiments have shown that a WSS of approximately 8 $\mathrm{dyn/cm}^2$ (using the viscosity of blood plasma and a wall shear rate of 500 s^{-1}), is usually enough to prevent significant platelet deposition (Navitsky et al. 2014), which is in line with the maximum surface stress calculated by Taylor et al. (2014): 5–10 $\mathrm{dyn/cm}^2$. Therefore, the breakdown thresholds for a thrombus at a domain boundary and at the thrombus surface are defined as 8 and 9 $\mathrm{dyn/cm}^2$, respectively, near the upper end of the maximum surface stress range. The constant defining the breakdown rate of a thrombus, B, is tentatively estimated from the breaking rate of platelet–platelet links established during preliminary simulations (Samra 2011) using Fogelson's (1992) model.

Table 1 Thrombosis model parameter values and sources

Parameter	Value	Source
D_n	1.58×10^{-7} cm^2/s	Goldsmith and Turitto (1986)
D_a	1.58×10^{-7} cm^2/s	Goldsmith and Turitto (1986)
D_{ADP}	2.37×10^{-6} cm^2/s	Hubbell and McIntire (1986a)
C	1.4854×10^{-7}	Soares et al. (2013)
α	1.4854	Soares et al. (2013)
β	1.4401	Soares et al. (2013)
k	9.56×10^{-12} cm^2	Adolph et al. (1997)
A	3×10^{-17} mol	Holmsen and Weiss (1979)
α_ε	3.7×10^{-5} cm^3/s	Empirical (Taylor et al. 2014)
B	2000 s^{-1}	Samra (2011)
ADP_t	2 μM	Frojmovic et al. (1994)
t_{ADP}	1 s	Sorensen et al. (1999a)
$\tau_{low,wall}$	0.2 dyn/cm^2	Empirical (Taylor et al. 2014)
$\tau_{high,wall}$	1.5 dyn/cm^2	Empirical (Taylor et al. 2014)
$\tau_{breakdown,wall}$	8 dyn/cm^2	Empirical (Navitsky et al. 2014)
$\tau_{low,thrombus}$	1 dyn/cm^2	Empirical (Taylor et al. 2014)
$\tau_{high,thrombus}$	3 dyn/cm^2	Empirical (Taylor et al. 2014)
$\tau_{breakdown,thrombus}$	9 dyn/cm^2	Empirical (Taylor et al. 2014)

The left column displays the symbol for all constants in the presented thrombosis model, the center column displays their value, and the right column gives the source for the given value. The term 'Empirical' in the right column indicates that the given value is either calculated or inferred based on experimental data contained within the cited source

2.2 In vitro experiments

Taylor et al. (2014) describe the experimental procedure used to generate the in vitro thrombus size and WSS data used in the model development; however, important details are reproduced here for completeness.

2.2.1 Blood collection and preparation

Bovine blood is drawn into 450-mL bags, each containing 63 mL of CPDA-1 anticoagulant. Blood is kept at room temperature and is used within four hours of collection to maximize platelet viability (Gottschall et al. 1986; Holme and Heaton 1995). Immediately preceding an experiment, the blood is recalcified with a calcium chloride solution to reverse the effect of the anticoagulant.

2.2.2 Blood circulation

The recalcified whole bovine blood is circulated through an acrylic, cylindrical backward-facing step (BFS) geometry, essentially, an asymmetric sudden expansion from a truncated circular cross section to a circular cross section, that produces well-defined flow separation. The step height is 2.5 mm—one quarter of the downstream vessel diameter. A peristaltic pump drives blood through a closed flow loop at a constant upstream Reynolds number (Re) of 490, maintaining laminar flow. Circulation times of 10, 15, 20, 25, 30, 45, 60, and 90 min are considered (5 min of blood circulation did not produce noticeable thrombus deposition), and after the desired time is reached ($n = 3$ for each), the blood is displaced with a phosphate-buffered saline (PBS) solution to provide contrast for MRI.

2.2.3 Magnetic resonance imaging

Standard 3D gradient echo sequences on a 7 T horizontal preclinical MRI system (Agilent, Santa Clara, CA, USA) are used to collect topographic information of the formed thrombi in stagnant PBS. The scans require 15 min to complete and result in an isotropic resolution of 150 μm (6 % of the step height). The final voxel resolution is reduced to 75 μm by applying zero filling (factor of two) in each direction.

2.2.4 Data processing and analysis

Thrombus size information is extracted from the MRI data through image segmentation. Four size metrics (thrombus height, length, exposed surface area, and volume) are measured to quantify thrombus growth, and the surface information extracted after segmentation is also used to exe-

cute CFD simulations on realistic thrombus geometries with the open-source CFD toolbox OpenFOAM (OpenCFD, Ltd, Bracknell, UK). The simulations are used to estimate how the WSS distribution on a thrombus surface changes as it grows into the model lumen.

2.3 Computational methods

OpenFOAM is used for meshing and thrombosis model simulations. Two-dimensional, structured meshes of hexahedral cells are created using the blockMesh utility in OpenFOAM that are equivalent to the centerline cross section of the three-dimensional BFS geometry from the in vitro thrombus size study used to develop the presented thrombosis model (Taylor et al. 2014).

The computational domain used to simulate thrombosis consists of a 10-mm-long channel with a height of 7.5 mm and an asymmetric sudden expansion to a 50-mm-long channel with a height of 10 mm, resulting in a step height of 2.5 mm (Fig. 3). The thrombosis model governing equations are incorporated into an existing OpenFOAM solver, which uses the finite volume method and the pressure implicit with splitting of operator (PISO) algorithm to calculate the pressure and velocity fields. At each computational time step, the following procedure is completed: (1) The pressure and velocity fields are updated using the aggregation intensity field from the previous time step, (2) all species concentrations are updated using the velocity field from the current time step, (3) the aggregation intensity field is updated using the current velocity field and species concentrations, and (4) the simulation advances to the next time step. All simulations are run in parallel on a single desktop computer.

Initial residuals for all variables are monitored and observed to drop at least three orders of magnitude (some up to eight orders of magnitude) within the first minutes of simulated blood flow. Simulation results are visualized using the open-source software ParaView (Kitware, Clifton Park, NY). Within ParaView, thrombus height (at the expansion), thrombus length, and the mean normalized aggregation intensity (mean aggregation intensity within the thrombus divided by the aggregation intensity threshold) are used to quantify thrombosis.

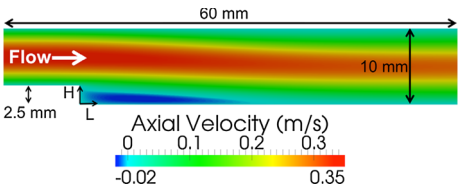

Fig. 3 Initial velocity field and domain dimensions used for all thrombus growth simulations. Axial velocity is illustrated using a *color map*, and the scale is nonlinear to accentuate the reversed flow (*dark blue*, with zero velocity shown as *light blue*) downstream of the asymmetric sudden expansion. Flow is from *left* to *right*, and coordinate axes indicate the direction for measurement of thrombus height (*H*) and length (*L*)

2.3.1 Validation of computational methods

A 2D domain with a step height of 4.9 mm and an upstream channel height of 5.2 mm, which matches the dimensions used in previous work, is used to validate the computational methods. In this geometry, the normalized reattachment length (length of recirculation region divided by the step height) is calculated for a range of laminar Reynolds numbers (Re): 150–750 and compared with previously published results (Guj and Stella 1988; Sohn 1988; Williams and Baker 1997). The present computations agree well over the entire range of Re.

2.3.2 Time step and mesh independence

Before comparing the model predictions of thrombosis to in vitro data, preliminary simulations are used to check for time step and mesh independence. Three two-dimensional meshes are generated for these tests, consisting of coarse, medium, and fine refinement levels. The meshes have isotropic cell dimensions of 312.5, 208.3, and 138.9 μm, respectively, in the plane of the simulations (a refinement factor of 1.5) and 5888, 13,248, and 29,808 computational cells, respectively. For comparison, the MRI scans used to generate the in vitro data set used in the model development had an isotropic spatial resolution of 150 μm (Taylor et al. 2014).

Simulations with time steps from 1 μs to 1 s are completed on the fine mesh, keeping all other parameters constant. Predicted thrombus growth is then compared between all simulations to check for time step independence. Likewise, three simulations are performed (one for each mesh refinement level) to check for mesh independence. Again, predicted thrombus growth, quantified as the mean normalized aggregation intensity in the domain, is used to compare the results from the different meshes. Richardson extrapolation quantifies the discretization error after thirty minutes of simulated thrombus growth, which is reported as a grid convergence index (GCI). The GCI, proposed by Roache (1994), relies on a factor of safety (1.25 in this case) to ensure that the GCI provides a reliable upper bound on the relative discretization error.

2.3.3 Model sensitivity to inlet concentration of activated platelets

As significant platelet activation is not expected to occur under laminar flow conditions, the primary determinants of the concentration of activated platelets in the computational

domain are the boundary and initial conditions, specifically the initial/background concentration of activated platelets. A small percentage of the total platelet population will be activated by the blood collection and handling procedures in an in vitro experiment, but this percentage may vary widely between research groups, with reported values from 1 % (Goodman et al. 2005) to nearly 20 % (Kennedy et al. 1997). Therefore, it is important to determine how changes in the background level of platelet activation affect simulated thrombus growth.

To accomplish this, the thrombosis model is non-dimensionalized using characteristic values for all dimensional variables. Particular attention is given to the equation for aggregation intensity, Eq. (11), as this equation contains a term to quantify thrombus deposition and growth. Equation (11) is non-dimensionalized using the average inlet velocity (U), step height (h), initial/background concentration of activated platelets ($\phi_{a,i}$), and the threshold aggregation intensity (ε_t), resulting in Eq. (14), where asterisks are used to denote dimensionless variables and operators.

$$\frac{\partial \varepsilon^*}{\partial t^*} + \left(\boldsymbol{u}^* \cdot \nabla^*\right) \varepsilon^* = \frac{h}{U} \cdot \frac{\alpha_\varepsilon P\left(\tau_w\right) \phi_{a,i}^2}{\varepsilon_t} \left(\phi_a^*\right)^2 - \frac{h}{U} \cdot \beta_\varepsilon\left(\tau_w\right) \varepsilon^* \tag{14}$$

The non-dimensional group that gives a measure of thrombus deposition and growth can be broken down into a characteristic flow time, h/U, and the inverse of a characteristic growth time (t_G), $\alpha_\varepsilon \phi_{a,i}^2/\varepsilon_t$ (assuming $P = 1$). While α_ε is calculated from in vitro data, the aggregation intensity threshold has no prescribed value. A preliminary set of simulations is run with background activated platelet percentages of 1, 5, 10, and 20 %. The corresponding aggregation intensity thresholds are varied to maintain a constant characteristic growth time (displayed in Table 2). For this analysis, a characteristic growth time of 216 s (chosen from preliminary simulations to produce realistic thrombus growth when compared to the in vitro data and calculated using a constant value of 1 for P) is used in all simulations to establish that t_G is the dominant predictor of thrombus growth rate.

Table 2 Parameter values to test model sensitivity to background level of platelet activation

Percent activation	$\phi_{a,i}$ ($\times 10^6$ platelets/mL)	$\phi_{n,i}$ ($\times 10^6$ platelets/mL)	ε_t ($\times 10^{12}$ cm^{-3})	t_G (s)
1	5	495	0.2	216
5	25	475	5	216
10	50	450	20	216
20	100	400	80	216

The percent activation and aggregation intensity threshold are varied in such a way that the characteristic thrombus growth time remains constant

A series of simulations is also run for different characteristic growth times to determine how background platelet activation affects predicted thrombus growth. This is done in two ways: (1) keeping the aggregation intensity threshold constant and varying the background activated platelet concentration and (2) maintaining a 5 % level of background platelet activation and varying the aggregation intensity threshold. A total of five simulations are run, and the parameter values used in each simulation are displayed in Table 3.

2.3.4 Thrombus growth simulations and comparisons to in vitro data

As mentioned previously, the thrombosis model is run using OpenFOAM, and blood flow is simulated for 30 min. The kinematic viscosity is defined as 3.5 cSt to match the asymptotic viscosity of whole bovine blood measured experimentally by Taylor et al. (2014). A steady, parabolic inlet velocity profile is imposed with a mean velocity of 0.229 m/s (Re = 490) to match the Re of the in vitro thrombus growth study used in the model formulation (Taylor et al. 2014), and flow is allowed to reach a steady-state solution before the thrombosis model is started (Fig. 3). At this Re, flow is within the laminar flow regime (Re < 1200) defined by Armaly et al. (1983) for an asymmetric sudden expansion. A constant pressure of zero is defined at the outlet, with zero gradient conditions specified at the inlet and outlet for pressure and velocity, respectively. No slip boundary conditions are used at all domain walls, and platelets are the only species to have nonzero inlet boundary conditions (and nonzero initial conditions throughout the computational domain). The total platelet population is approximated as 500×10^6 platelets/mL to match bovine blood (Soloviev et al. 1999), with an estimated 5 % level of background activation. This results in constant inlet and initial values of 475×10^6 and 25×10^6 platelets/mL for non-activated and activated platelets, respectively. Aggregation intensity thresholds of 3–7×10^{12} cm^{-3} are considered. Thrombus height and length are then compared to the in vitro thrombus size data for increasing time to check for agreement. Additionally, the computational results are analyzed to look at how the activated platelet population and fluid shear stress distribution change with increasing time.

2.3.5 Thrombosis model validation

The thrombosis model is developed (Sect. 2.1.6) with the same in vitro data (Taylor et al. 2014) that is later used to check the model predictions (Sect. 3.3). Therefore, indepen-

Table 3 Parameter values to test model sensitivity to characteristic thrombus growth time

Simulation number	Percent activation	$\phi_{a,i}$ ($\times 10^6$ platelets/mL)	$\phi_{n,i}$ ($\times 10^6$ platelets/mL)	ε_t ($\times 10^{12}$ cm^{-3})	t_G (s)
1	2.5	12.5	487.5	5	865
2	5	25	475	2.5	108
3	5	25	475	5	216
4	5	25	475	7.5	324
5	7.5	37.5	462.5	5	96

Five different characteristic thrombus growth times are examined, and they have been assigned a simulation number between 1 and 5. The background platelet activation level and aggregation intensity threshold for each simulation are also given

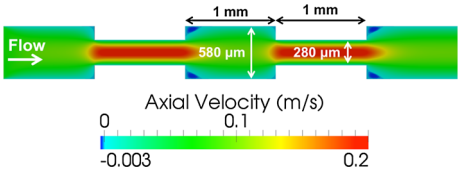

Fig. 4 Initial velocity field and domain dimensions used for thrombosis model validation simulations. The dimensions match the centerline of a flow cell used by Goodman et al. (2005) for in vitro thrombosis experiments. Axial velocity is illustrated using a *color map*, and the scale is nonlinear to accentuate reversed flow (*dark blue*, with zero velocity shown as *light blue*). Flow is from *left* to *right*

dent experiments must be used to truly test the predictive power of the thrombosis model. Unfortunately, quantitative studies of macroscopic thrombus growth are not readily available; however, Goodman et al. (2005) present locations of in vitro thrombus deposition, detected with scanning electron microscopy (SEM) and video microscopy (VM), in a flow cell consisting of polyethylene sudden contractions and expansions (see Fig. 4), which they use to validate portions of their own thrombosis model. The geometry alternates between large and small tubing segments (inner diameters of 580 and 280 μm, respectively), with each segment being 1 mm in length, and heparinized blood is perfused through the flow cell at a constant flow rate of 0.75 mL/min.

The same numerical methods described earlier are used in the validation simulation, with a few notable exceptions. Goodman et al. (2005) used human blood and, consequently, the total platelet population is estimated to be 300×10^6 platelets/mL. Accordingly, the dynamic viscosity and density are defined as 3 cP and 1060 kg/m^3, respectively, and background platelet activation is set at 1 % to match their experiments. A 2D uniform mesh, equivalent to the centerline of the in vitro model of symmetric expansions and contractions, is generated with an isotropic cell size of 10 μm (a total of 23,000 mesh elements). Finally, blood flow is simulated for thirty seconds using time steps of 1 ms. A parabolic velocity profile (mean velocity = 0.047 m/s) is imposed at the inlet to match the experimental conditions, resulting in an inlet Re of 9.6. Reported WSSs (Goodman et al. 2005) are compared to those calculated in the present simulations to ensure simulation accuracy.

3 Results

3.1 Time step and mesh independence

The thrombosis model is determined to be independent of the computational time step for all time steps that give a stable solution. On the fine mesh, time steps greater than or equal to 50 ms do not provide stable solutions; however, using time steps of 10 ms or less results in solutions that agree with each other within 5 %. Hence, the largest time step that results in stable solutions on the fine mesh (10 ms) is used for all other meshes.

We find simulated thrombus growth on the fine mesh has a sufficiently small discretization error to ensure simulation results would not be substantially different on a more refined mesh, as established by calculating the GCI after 30 min of thrombus growth. The GCI, and thus the upper bound on relative discretization error, is 15 % on the fine mesh, and accordingly, the fine mesh is used for the rest of the presented BFS results.

3.2 Sensitivity to platelet activation percentage

There is no difference in predicted thrombus growth when simulations using the values of platelet activation from Table 2 are compared with each other, confirming the importance of t_G to the computational results. After establishing the importance of t_G, the effect of varying t_G is investigated by plotting the results of the simulations using the parameter values from Table 3 in Fig. 5. Large differences in predicted thrombus growth are observed when the characteristic growth time is varied, as illustrated in Fig. 5a, b. After comparing all five simulations, it is apparent that the predicted rate of thrombus growth is inversely proportional to t_G. For instance, Simulation 1 ($t_G = 865$ s) predicts the slowest thrombus growth, with the thrombus reaching a size after 30 min of simulated blood that Simulation 5 ($t_G = 96$ s) pre-

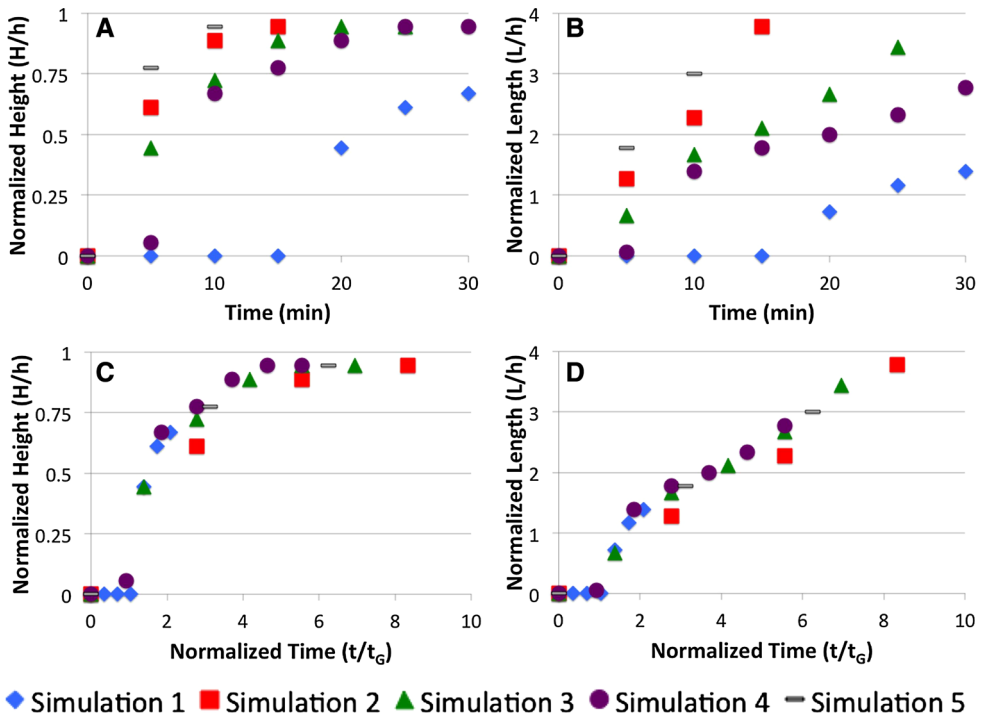

Fig. 5 Results of the sensitivity analysis performed with the five simulations from Table 3 are displayed for the first 30 min of simulated blood flow. Thrombus height (H) and length (L) are normalized using the step height (h) of 2.5 mm. Large discrepancies are observed in the rate of predicted thrombus growth for both **a** height and **b** length; however, the respective characteristic growth times for the five simulations can be used to normalize time and collapse all the curves for each size metric to one: **c**, **d**

dicts in <5 min. However, the two simulations with similar characteristic growth times, Simulations 2 ($t_G = 108$ s) and 5 ($t_G = 96$ s) produce similar results, although Simulation 5 does predict slightly faster growth.

To determine whether the differences in predicted thrombus growth between the five simulations from Table 3 are primarily due to differences in their respective characteristic growth times, thrombus growth is re-examined using "normalized time," which is simply time divided by t_G. When the time axes are normalized using the respective characteristic growth time for each simulation, the five separate growth curves collapsed to one for both thrombus height (Fig. 5c) and length (Fig. 5d).

3.3 Thrombus growth simulations and comparisons to in vitro BFS data

After performing simulations with aggregation intensity thresholds from 3 to 7×10^{12} cm^{-3} and comparing the results with the in vitro data of Taylor et al. (2014), we found an aggregation intensity value of 5.25×10^{12} cm^{-3} provides the best agreement to the in vitro results ($t_G = 206$ s). Predicted thrombus height and length are normalized using the step height and are plotted with the in vitro data in Fig. 6. The computational results are generally within the expected range based on 95 % confidence intervals from the in vitro data. A thrombus first appeared between 4 and 5 min into the simulation, in agreement with the in vitro data—a thrombus was not detected in the MRI scans until between 5 and 10 min into blood circulation. Thrombus deposition occurs at the expansion and at the reattachment point; however, the MR scans only detected a measureable thrombus at the expansion. Consequently, only the thrombus at the expansion is compared to the in vitro data. In Fig. 6a, the simulated thrombus height rapidly increases between 5 and 10 min into the simulation and reaches a maximum normalized value of 0.94, nearly the step height, after 19 min of simulated time. Likewise, the in vitro thrombi reach an asymptotic height after 15–20 min of blood flow. Figure 6b shows similar agreement. The one exception is thrombus length at 25 min, with the in vitro length being significantly greater than the thrombosis model prediction. However, the two data sets are again in agreement after 30 min of blood flow.

Figure 7a provides a qualitative look at the simulated thrombus growth plotted in Fig. 6 and focuses on thrombus growth at the corner after the expansions. The simulated thrombus grows into the lumen of the model, occupying nearly the entire initial recirculation region after 30 min. No results are presented after 30 min, as this is when the throm-

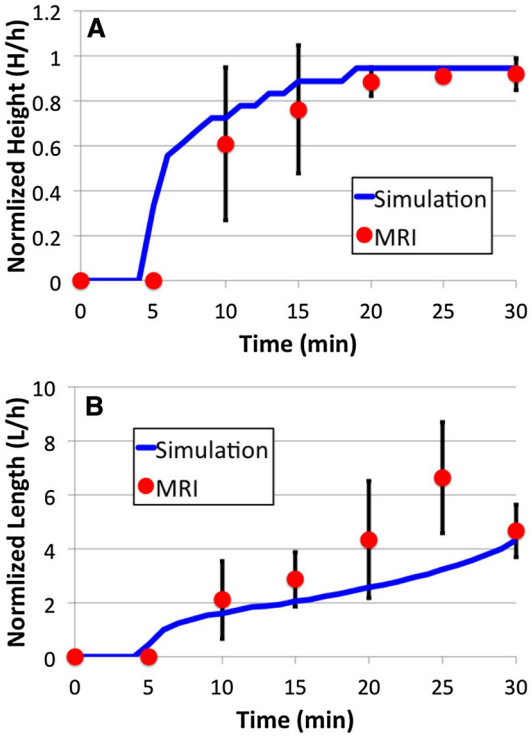

Fig. 6 Results of the simulation using an aggregation intensity threshold of $5.25 \times 10^{12}\,\mathrm{cm}^{-3}$ plotted with the in vitro growth data obtained with MRI (Taylor et al. 2014). The in vitro results are presented as a mean value with error bars denoting the 95 % confidence interval. Normalized thrombus **a** height and **b** length are plotted for the first 30 min of blood flow. All values are normalized using the step height

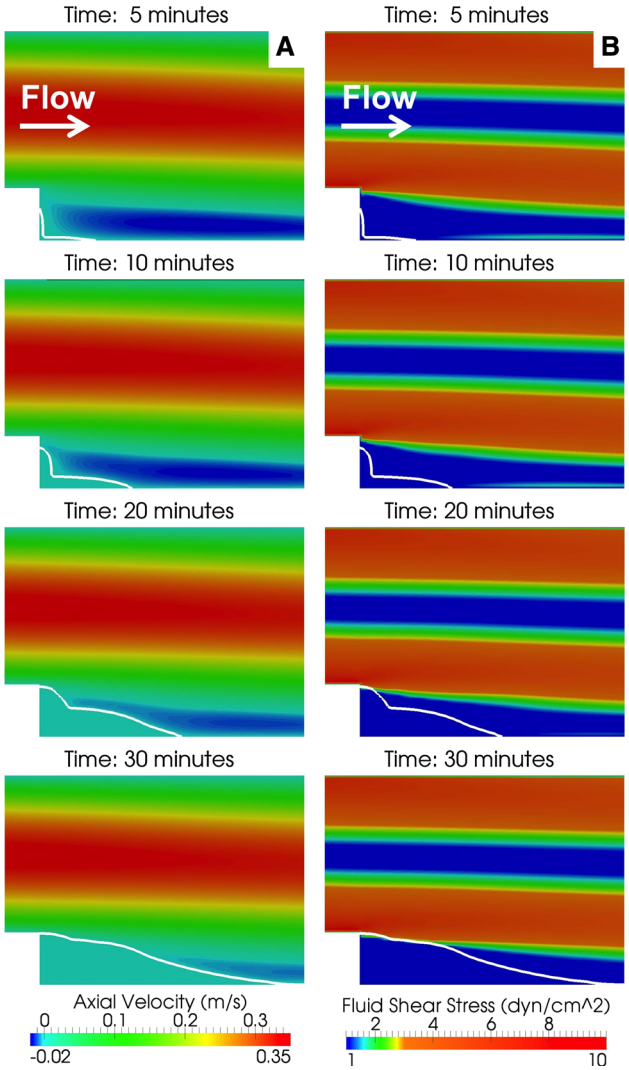

Fig. 7 **a** Simulated thrombus growth for times from 5 to 30 min is visualized with a *white contour line* based on the aggregation intensity threshold. A nonlinear *color map* shows axial velocity, with the color scale compressed near zero to better show areas of flow reversal (*dark blue*, with zero velocity shown as *light blue*). A thrombus forms in the corner after the sudden expansion and grows into the lumen and downstream, away from the expansion. The thrombus grows into the recirculation region, causing it to shrink and nearly disappear after 30 min. Flow is from left to right. **b** Fluid shear stress, calculated using the magnitude of the local velocity gradient, is presented with increasing time. The color scale has been adjusted so all shear stresses above $3\,\mathrm{dyn/cm}^2$ are shown as *red*, as this is maximum shear stress at which thrombus growth can occur in the model. The outlines of growing thrombi are given as *solid white lines*, and flow is from *left* to *right*

bus at the expansion and at the reattachment point merge and render comparisons with the in vitro data invalid. One simulation is run longer, and only slow growth downstream (at a rate of $<0.5\,\mathrm{mm/min}$) is predicted after the thrombi merge. Figure 7b complements Fig. 7a by illustrating how the fluid shear stress field changes throughout the domain with increasing time, as thrombus deposition and growth is dictated by a weighting function, Eq. (12), that depends on the local WSS. Initially, for simulated times up to 15 min, the thrombus near the expansion has its entire surface within the recirculation region, leading to rapid thrombus growth into the lumen and downstream. After 20 min, the thrombus near the expansion still has most of its surface within the recirculation region, but the most upstream portion approaches regions of high velocity and consequently experiences surface shear stresses that exceed the $3\,\mathrm{dyn/cm}^2$ threshold, preventing additional deposition to that region. By 30 min, the entire upstream thrombus boundary near the expansion experiences surface stresses exceeding the maximum deposition threshold; however, there are still downstream locations on the thrombus surface with nearby flow reversal and low shear stresses, which allow further growth. The maximum shear stress near the thrombus surface after 30 min of simulated time is $4.4\,\mathrm{dyn/cm}^2$, while the average surface shear stress is approximately $0.9\,\mathrm{dyn/cm}^2$. For comparison, the maximum surface shear stress on the in vitro thrombi formed after 30 min ($n = 3$) was $6.1 \pm 2.6\,\mathrm{dyn/cm}^2$ (mean $\pm$ SEM) and the average surface shear stress was $0.64 \pm 0.4\,\mathrm{dyn/cm}^2$ (Taylor et al. 2014).

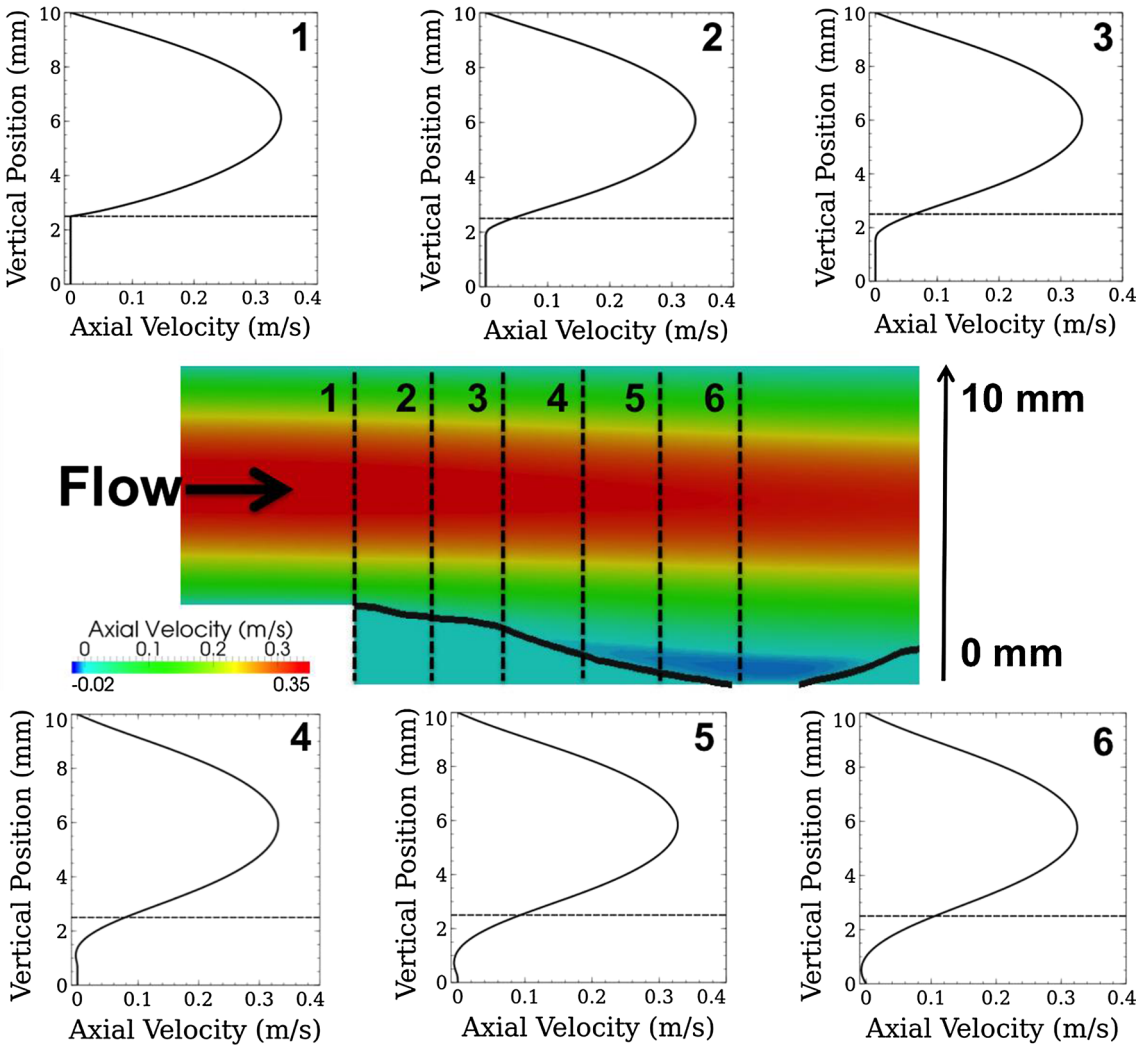

Fig. 8 Six axial velocity profiles taken after 30 min of simulated thrombus growth. The profiles start at the expansion and proceed downstream with a spacing of 2.5 mm, the step height. The locations of the six profiles are illustrated with *dashed lines* through the *color plot* and labeled numerically to the *left* of the *line*. Each profile is taken vertically through the computational domain, with a vertical position of 0 mm at the lower wall and 10 mm at the upper wall. The axial velocity profiles are shown in *solid black lines* in plots *1–6*, with the step height displayed at a constant vertical location of 2.5 mm using a *dashed line*. Flow is from *left* to *right*

While velocity patterns and magnitudes are qualitatively displayed in Fig. 7a near a formed thrombus, Fig. 8 provides a quantitative perspective. Six velocity profiles are presented, starting at the expansion and moving downstream in increments of the step height (2.5 mm). Starting with velocity profile 1, all velocity below the step height is zero and the profile is centered at a vertical location of 6.25 mm (the center of the upstream channel) with a maximum velocity of 0.343 m/s (1.5 multiplied by the average inlet velocity). In velocity profile 3, the maximum velocity has dropped slightly to 0.335 m/s at a vertical location of 6 mm. Velocity profiles 4–6 all show flow reversal (also shown as dark blue regions in the color plot), and the maximum velocity decreases to 0.325 m/s at a vertical location of 5.8 mm in velocity profile 6, as the velocity field adjusts to the wider channel.

Even though flow remains laminar throughout the computational domain, there is still mechanical activation of platelets, which is visualized using a normalized percent increase of activated platelets—a measure of the increase in activated platelets above the background level (Fig. 9). Initially, small increases are observed in the recirculation region due to activated platelets becoming trapped in the recirculating fluid. The heightened concentration of activated platelets in the recirculation region leads to an increased thrombus growth rate in the nearby regions of low WSS, and normalized increases up to 10 % above the background level are calculated within the simulated thrombus after thirty minutes.

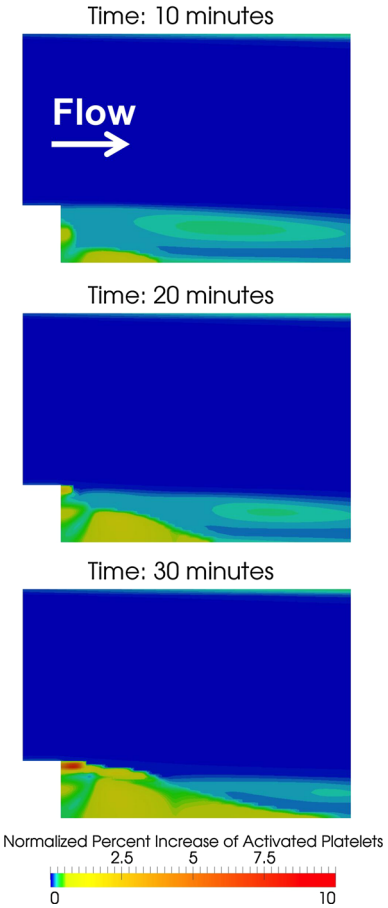

Fig. 9 Normalized percent increase in the concentration of activated platelets $[100 \times (\phi_a - \phi_{a,i}) / \phi_{a,i}]$ is shown using a color map (zoomed in on the portion of the computational domain near the expansion), which provides a measure of the increase in activated platelets above the background level. Heightened concentrations of activated platelets are initially observed in the recirculation downstream of the expansion, which persists throughout the simulation. In addition, elevated amounts of activated platelets are seen within growing thrombi. The color scale has been compressed near zero to better illustrate small changes in the concentration of activated platelets above the background level. Flow is from *left* to *right*

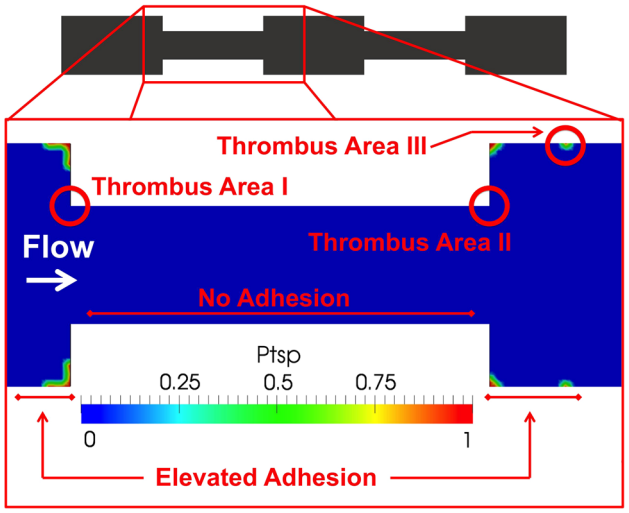

Fig. 10 Locations of predicted thrombus deposition, quantified using P_{TSP}, in a portion of the flow cell shown in Fig. 4. The three areas of in vitro thrombus deposition highlighted by Goodman et al. (2005) are indicated with *circles*. In addition to the three primary areas, Goodman et al. (2005) also note substantial deposition upstream and downstream of the contractions in their SEM and VM images, including in the *corners*, with nearly no deposition in the contractions (indicated along the bottom model wall). Flow is from *left* to *right*

3.4 Thrombosis model validation

The thrombosis model is used to estimate locations of potential thrombus deposition in a 2D representation of the in vitro flow cell of Goodman et al. (2005). The flow through the model, particularly WSS, is compared to the reported values to ensure simulation accuracy. In the small and large diameter segments, Goodman et al. (2005) report WSSs of 174 and 19.6 dyn/cm^2, respectively. The present simulations have a WSS of 183.6 dyn/cm^2 at the leading portion of the small segments and a WSS of approximately 21.5 dyn/cm^2 in the large segments (differences of $<10\,\%$ in both cases). Figure 10 illustrates predicted locations of thrombus deposition through a plot of P_{TSP} in the computational domain, and the in vitro locations of thrombus deposition highlighted by Goodman et al. (2005). The thrombosis model predicts initial thrombus deposition in the corners of both the sudden contractions and expansions and also at the reattachment point downstream of the expansions (Fig. 4). Goodman et al. (2005) highlight three main locations of in vitro thrombus deposition (Fig. 10): at the entrance and exit of the small segments and at the reattachment point downstream of the sudden expansions; however, their SEM and VM images also show evidence of significant deposition upstream and downstream of the contractions, including in the corners. Goodman et al. (2005) also note that while deposition is observed at the upstream and downstream corners of the small diameter sections (Thrombus Areas I and II in Fig. 10), there are almost no adherent platelets between the corners. Likewise, Fig. 10 shows no predicted deposition in the small diameter sections.

4 Discussion

The thrombosis model and results show promise for timely predictions of macroscopic thrombus growth under conditions relevant to cardiovascular device-induced thrombosis. The model represents a substantial simplification of the complex thrombotic process (Fig. 1), with only one cellular species (platelets) and one chemical species (ADP) retained from the large number in the full network; nevertheless, the predictions of the simplified model agree with in vitro thrombus growth data collected using whole blood (Fig. 5), as well

as with locations of thrombus deposition reported by an independent research group (Goodman et al. 2005) in a geometry consisting of sudden expansions and contractions (Fig. 10).

Computational time steps of 10 ms are used in presented simulations, which is possible due to the pseudo-steady nature of the flow field. The inlet flow is steady, and thrombus growth is slow enough that a formed thrombus is essentially constant in size over any two consecutive time steps. This is confirmed by the calculation of a range of characteristic thrombus growth times (Table 3), which are all orders of magnitude greater than the computational time step. These results are somewhat surprising, considering many of the underlying processes contributing to thrombosis occur over timescales <10 ms; however, many of these processes also occur on small spatial scales that are neglected in the model. These results provide evidence that accurate predictions of macroscopic thrombus growth do not require resolution of the shortest time scales involved in the thrombotic process.

Furthermore, the results of the grid refinement study provide evidence that even thrombosis simulations on coarse meshes can provide useful information to researchers. While the fine mesh was used for the presented results, the coarse mesh, consisting of only about 5000 computational cells (each with an area four orders of magnitude greater than a single platelet), produces results that have a percent error of approximately 40 % when compared to the true solution calculated with Richardson extrapolation. While these errors are too large for quantitative predictions of thrombosis, qualitative conclusions could still be drawn about locations and relative growth rates of thrombi. This bodes well for the eventual application of the thrombosis model to the three-dimensional geometries and pulsatile flow conditions of cardiac devices, where high levels of mesh refinement may prove to be computationally prohibitive. Moreover, even though the thrombosis model has only been used in two-dimensional geometries to date, all of the governing equations and numerical methods are transferable to three-dimensional geometries.

A latency period is observed in both the computational and in vitro growth plots, as a macroscopic thrombus does not appear until 5 min into the simulations and between 5 and 10 min in the MRI study. This is a direct result of neglecting the small spatial scales involved with thrombosis. The MR scans produce an initial voxel resolution of 150 μm, but a thrombus would presumably need to grow to at least 300 μm in size before it could be reliably detected during image processing. The thrombosis model requires the aggregation intensity in a computational cell to exceed a threshold value before that cell is considered to be part of a thrombus. As a result, the latency period in the simulations is caused by the time needed to increase the aggregation intensity in boundary cells to at least the threshold level before a thrombus is observed.

The thrombosis model predicts thrombus deposition in the corner downstream of the expansion and at the reattachment point of the recirculation region. Thrombus growth is compared to in vitro data (Taylor et al. 2014) for the first 30 min of blood flow in a simplified, 2D representation of the in vitro geometry, corresponding to the centerline of the backward-facing step. While this simplification may lead to small discrepancies between the in vitro and in silico flow patterns, we assume, for the purpose of model development, that steady and laminar flow ensures that the 2D domain still captures the main fluid mechanics phenomena, such as flow separation and reattachment, from the 3D geometry and that there is little out-of-plane flow in the 2D domain. Also, as the in vitro study only found thrombus growth at the expansion, and not at the reattachment point, any comparisons once the two simulated thrombi merged would not have been valid. Platelet adhesion and thrombus deposition have been seen at the reattachment point of separated flow regions by other researchers (Karino and Goldsmith 1979; Tamagawa et al. 2009); however, they were studying microscopic events or individual particles. As the MRI resolution was 150 μm (Taylor et al. 2014) for the visualization of thrombi used to develop the model, any small platelet aggregates at the reattachment point would not have been resolved. With all experimental studies, it is well known that the reattachment point will wander. Consequently, there would not have been a static point of zero WSS due to a constant reattachment length in the in vitro experiments as there is in the simulations, and the constant location of zero WSS is a major contributor to the predicted thrombus deposition at the reattachment point in the simulations.

Also, the in vitro thrombi reached asymptotic sizes after approximately 45 min of blood circulation (Taylor et al. 2014), while the thrombosis model predicts continuous, albeit slow, growth in the downstream direction for at least 120 min. This may be due to the boundary conditions of the simulations, where fresh platelets are continuously delivered into the domain. In contrast, blood was circulated through a closed loop for the in vitro experiments, which may have led to a depletion of platelets or other species in the coagulation cascade over time. Additionally, clotting properties of the bovine blood, such as the activated clotting time or platelet function, were not measured prior to, or after, the in vitro experiments. As such, the error bars for the in vitro data are likely the contribution of animal-to-animal variability. Nevertheless, some of this uncertainty is removed by conducting three experiments for each circulation time and by using the calculated 95 % confidence intervals to assess simulation accuracy. Additionally, even though the present work focuses on early thrombus growth ($\leq$30 min), which should lessen any disagreements between the simulations and MRI data caused by the assumption of a continuous supply of fresh blood to the computational domain, the thrombotic capability

of blood during the in vitro experiments was unknown and may have been compromised before the end of the experiments. Finally, as simulated species only make one pass through the computational domain, the degradation of ADP is neglected in Eq. (10), due to its half-life of 45 min (Goodman et al. 2005).

In Fig. 7a and profiles 2–5 in Fig. 8, it appears as though the velocity within the thrombi drops to zero due to the Brinkman term in Eq. (2); yet, the velocities never actually reach zero. However, they are small enough (10^{-9}–10^{-11} m/s) that any mass transport within the thrombus is dominated by diffusion. Of course, we only use one estimate of thrombus permeability in the present work, and a large range of permeabilities is likely found in vivo. Wufsus et al. (2013), for example, calculate permeabilities that span five orders of magnitude for clots formed from platelet-rich plasma with varying concentrations of platelets and fibrin, with permeabilities as high as 1.1×10^{-10} cm^2 for a platelet concentration of 700×10^6 platelets/mL, which may be more indicative of the white clots that form in the arterial circulation. However, even with more permeable thrombi, there will still be substantial resistance to flow within a formed thrombus, and we expect that predicted thrombus growth from our model is largely independent of thrombus permeability. However, increased thrombus permeability may lead to higher rates of chemical activation within formed thrombi under certain conditions, due to heightened transport of ADP into the thrombus.

Portions of the model development were made possible using in vitro data (Taylor et al. 2014), particularly the calculation of α_ε, the constant controlling the volumetric rate of thrombus deposition in Eq. (11). Additionally, some of the WSS thresholds for thrombus deposition, growth, and breakdown are determined empirically. First, WSS is used rather than wall shear rate in an attempt to make the model compatible with a range of fluid viscosities and potentially allow for the incorporation of a non-Newtonian fluid model in the future. Second, only an estimate for WSS thresholds is obtained from the MRI data set, and the estimated WSS thresholds for thrombus deposition to wall (i.e., adhesion) and thrombus deposition to an already formed thrombus (i.e., growth/cohesion) are set to different values, although both are near the empirical estimate. Justification for this is based on the fact that Sorensen et al. (1999b) determined the adhesion rate for activated platelets to a collagen surface was the same as the cohesion rate for activated platelets binding together. Furthermore, Hubbell and McIntire (1986b) presented results that indicate platelets can more easily adhere to a collagen surface than to either polyurethane or nylon. The in vitro BFS model was acrylic (Taylor et al. 2014), which is assumed to have blood-contacting properties closer to polyurethane or nylon than collagen. Consequently, the WSS threshold values for cohesion are defined slightly higher than the values for adhesion.

We have validated our WSS thresholds by comparing predicted thrombus deposition (Fig. 10) to reported locations in an in vitro flow cell of sudden expansions and contractions (Goodman et al. 2005). The only areas of disagreement are Thrombus Areas I and II, which are the entrance and exit regions of the small diameter sections (Fig. 10). However, the thrombosis model correctly predicts deposition, or lack thereof, at all other locations. Additionally, thrombi in the two areas our model did not correctly predict (Thrombus Areas I and II in Fig. 10) will likely never grow to more than tens of microns in height, which helps explain why our thrombosis model does not resolve them—they exist on a spatial scale that we do not endeavor to simulate. While these results do not validate predicted thrombus growth, and thus presented values of ε_t and α_ε, they do show the potential of the thrombosis model to provide realistic predictions of thrombus deposition in geometries and flow conditions outside of those used in the model development. Unfortunately, quantitative macroscopic thrombus growth data on spatial and temporal scales relevant to medical devices are lacking in the literature to fully validate our model, aside from the MRI study (Taylor et al. 2014) referenced in the model development. However, Folie and McIntire (1989) estimated average thrombus volume with increasing time in a parallel-plate flow chamber with whole blood, using collagen to initiate deposition. They employed three flow conditions for 150 s each, and one of their conditions (wall shear rate = 100 s^{-1}; corresponding to a WSS of 3.5 dyn/cm^2, assuming a dynamic viscosity of 3.5 cP) is close to the WSS found downstream of our asymmetric expansion. At their 100 s^{-1} condition, they found a final average thrombus volume of approximately 2250 μm^3 after 150 s, which can be used to estimate their volumetric growth rate: 1.5×10^{-5} cm^3/s. As Folie and McIntire (1989) acquired whole blood from a different mammal than us (human vs. bovine), used a different anticoagulant than us (heparin vs. CPDA-1), and conducted their experiments in a substantially different geometry than ours (parallel-plate flow chamber vs. an asymmetric sudden expansion), we find it reassuring that their average volumetric growth rate only differs from ours by a factor of approximately 2.5 (ours is 3.7×10^{-5} cm^3/s). Importantly, this gives us confidence that our model parameters will provide realistic thrombus growth rates under a range of flow and blood conditions and, when combined with our validation of thrombus deposition locations, provides evidence for the predictive power of our thrombosis model.

Also, an assumption is made for the calculation of WSS near a thrombus surface, namely that the magnitude of the Jacobian matrix composed of all components of the velocity gradient near the surface is dominated by the surface normal component. As thrombus surfaces are not explic-

itly tracked, surface normal vectors, and thus surface normal velocity gradients, are not available during the simulation, and the magnitude of the velocity gradient matrix is used instead. Validation that this is an acceptable assumption is provided by the fact that both mean and maximum shear stresses in computational cells on the thrombus surface after 30 min of simulated time are comparable to the values calculated using the true surface normal velocity gradients on the reconstructed surfaces of the in vitro thrombi after the same duration of blood circulation (Taylor et al. 2014).

The term for chemical activation of platelets in Eq. (7) requires a threshold concentration of ADP before any activation occurs. That threshold is never reached in the simulations due to low rates of platelet activation, and thus, low rates of ADP release. Still, there is platelet activation in the domain, which is caused solely by mechanical stimuli and quantified with Eq. (8). Even though the shear stresses throughout the model are low ($\leq$10 dyn/cm^2), there is no threshold shear stress required in the power law term for mechanical activation. Figure 9 shows that the maximum increase in the activated platelet population is about 10 % above the background level, and the increase is localized to the recirculation region and growing thrombi. These results show mechanical activation levels are not negligible, even in laminar flows, and it is important to include mechanical activation in models of device-induced thrombosis. Additionally, our results are comparable to those of a computational study by Hansen et al. (2015), where they considered both Lagrangian (which included stress histories of platelets) and Eulerian (which included a power law term similar to the one used in the thrombosis model) techniques to quantify mechanical platelet activation in patient-specific abdominal aortic aneurysm (AAA) geometries. They determined the amount of mechanical platelet activation was small when compared to background levels of platelet activation, and the two classes of techniques largely agreed with each other. Also, the phenomenon of activated platelets becoming trapped in a recirculation region and deposited to nearby regions of low WSS (Fig. 8) has been observed previously (Bluestein et al. 1996) and will likely play a larger role in thrombus formation and growth in conditions and geometries that promote greater amounts platelet activation above the background level.

Turbulent flow may be a way to generate platelet activation that significantly exceeds background levels. Currently, the model is not formulated to handle turbulence; however, modifications can likely be made in the future, such as the inclusion of Reynolds shear stress in the term for mechanical platelet activation, to make the model compatible with the high Reynolds number flows associated with some blood-contacting devices, such as heart valves and ventricular assist devices. Turbulent flow, along with pulsatility, would also likely increase the chances of embolization. Presently, an initial guess is made at B, the thrombus breakdown rate, but due to steady and laminar conditions, this term is never activated in current work. While the MRI experiments were not designed to detect embolization, we do not believe any significant embolization occurred. This is based on visual inspections of thrombi after experiments and embolization probability maps developed by Basmadjian (1989). First, all thrombi appeared similar in shape and did not show evidence of significant embolization (Taylor et al. 2014). Second, only the largest thrombus protrusions in the MRI study entered the transitional risk region of the embolization probability maps, 25–75 % chance of embolization (Basmadjian 1989), based on CFD results (Taylor et al. 2014). The vast majority of thrombus surface protrusions fell into the low-risk region of embolization (<25 % chance of embolization). We anticipate that there will be a much higher probability of embolization if pulsatile flow is used, due to the simulated thrombus surface experiencing heightened shear stress during portions of the flow cycle. The present thrombosis model is currently formulated with only steady and laminar conditions in mind, and as a result, future modifications to the model, particularly the improvement of thrombus breakdown and the inclusion of macroscopic embolization, must be made before thrombosis is simulated in the highly pulsatile, and likely turbulent, flows of the arterial circulation.

Toward the eventual goal of improving cardiovascular device development, predictions of thrombus formation and growth in the time domain may not be important, only the locations of thrombus deposition and estimates of their eventual size. The sensitivity analysis (Table 3) shows the dependence of predicted thrombus growth on background platelet activation and aggregation intensity threshold can be eliminated by normalizing the time variable with the characteristic thrombus growth time (Fig. 5), providing information on thrombus location and size to researchers without any dependence on background platelet activation caused by the blood-handling protocols of individual research groups. If the thrombosis model is used to optimize potential device geometries or operating conditions before in vitro or in vivo trials, accurate predictions of thrombus location and size, regardless of formation time, should still prove useful.

The next logical step in the development of our thrombosis model is to simulate thrombus growth in three dimensions, which will allow us to better reproduce the fluid velocities that dictate thrombus deposition and growth in our model. With additional in vitro experiments, we can quantitatively validate advanced thrombus growth metrics, such as thrombus surface area and volume, in an effort to further demonstrate the predictive power of our model.

5 Conclusions

We have developed and presented a computational model for macroscopic predictions of cardiovascular device-induced thrombosis. Assuming fluid mechanics are the dominant predictor of device-induced thrombosis, the thrombotic process is simplified to the network displayed in Fig. 1. The network includes the bulk concentrations of three species: non-activated platelets, activated platelets, and ADP; additionally, a scalar "aggregation intensity" is tracked to quantify a growing thrombus and couple it with the local field through a modified Brinkman term in the Navier–Stokes equations. Locations of thrombus deposition and the rate of thrombus growth are determined with the novel use of a WSS-dependent term, and both chemical and mechanical platelet activation are considered. When the model sensitivity to background levels of platelet activation is tested, predicted thrombosis is determined to be largely independent of the background concentration of activated platelets, as long as the characteristic thrombus growth time is used to normalize the time variable (Fig. 5). Simulations are performed in an asymmetric sudden expansion that produces flow separation relevant to blood-contacting devices, and thrombi are predicted to form in the recirculation region downstream the step and near the reattachment point (Fig. 7a). Subsequently, they grow into nearby low shear regions (Fig. 7a, b), and thrombus growth downstream of the expansion is enhanced by the capture of activated platelets by the recirculating flow (Fig. 9). In contrast with earlier models, the current model uses a data set of time-dependent thrombus size collected in vitro with MRI (Taylor et al. 2014) to help develop the model and quantitatively evaluate its predictions of macroscopic thrombus growth. The computational results agree well with the in vitro data when thrombus height and length are compared for 30 min of blood flow (Fig. 5). Furthermore, locations of thrombus deposition are validated against the in vitro work of an independent research group in Fig. 10 (Goodman et al. 2005).

As the presented results, which rely on a greatly simplified network of the thrombotic process, agree with in vitro thrombus growth data collected using whole blood, it is reasonable to conclude that the fluid mechanics of the system is the dominant predictor and controlling factor of thrombus formation and growth in the regions of separated flow relevant to cardiovascular devices. Crucially, this bodes well for the continuing development of our model and its eventual application to the complex and three-dimensional geometries and flows associated with blood-contacting devices, which are ill suited for any of the existing thrombosis models. Our thrombosis model can help researchers better understand how the fluid mechanics of devices contribute to thrombosis, and with future validation under pulsatile conditions and the incorporation of more clinically relevant materials, it can help optimize and expedite the device development process.

Acknowledgments A Walker Graduate Assistantship from the Applied Research Laboratory at the Pennsylvania State University and a Penn State Grace Woodward Foundation grant supported this work.

References

Adolph R, Vorp DA, Steed DL, Webster MW, Kameneva MV, Watkins SC (1997) Cellular content and permeability of intraluminal thrombus in abdominal aortic aneurysm. J Vasc Surg 25(5):916–926. doi:10.1016/S0741-5214(97)70223-4

Armaly BF, Durst F, Pereira JCF, Schonung B (1983) Experimental and theoretical investigation of backward-facing step flow. J Fluid Mech 127:473–496. doi:10.1017/S0022112083002839

Basmadjian D (1989) Embolization: critical thrombus height, shear rates, and pulsatility. Patency of blood vessels. J Biomed Mater Res 23(11):1315–1326. doi:10.1002/jbm.820231108

Bludszuweit C (1994) A theoretical approach to the prediction of haemolysis in centrifugal blood pumps. Dissertation, University of Strathclyde

Bluestein D, Niu L, Schoephoerster RT, Dewanjee MK (1996) Steady flow in an aneurysm model: correlation between fluid dynamics and blood platelet deposition. J Biomech Eng 118:280–286. doi:10.1115/1.2796008

Cito S (2013) Review of macroscopic thrombus modeling methods. Thromb Res 131:116–124. doi:10.1016/j.thromres.2012.11.020

Fogelson AL (1992) Continuum models of platelet aggregation: formulation and mechanical properties. SIAM J Appl Math 52(4):1089–1110. doi:10.1137/0152064

Fogelson AL, Guy RD (2008) Immersed-boundary-type models of intravascular platelet aggregation. Comput Methods Appl Mech Eng 197:2087–2104. doi:10.1016/j.cma.2007.06.030

Folie BJ, McIntire LV (1989) Mathematical analysis of mural thrombogenesis: concentration profiles of platelet-activating agents and effects of viscous shear flow. Biophys J 56(6):1121–1141. doi:10.1016/S0006-3495(89)82760-2

Frojmovic MM, Mooney RF, Wong T (1994) Dynamics of platelet glycoprotein IIb–IIIa receptor expression and fibrinogen binding. I. Quantal activation of platelet subpopulations varies with adenosine diphosphate concentration. Biophys J 67:2060–2068. doi:10.1016/S0006-3495(94)80689-7

Gear AR (1982) Rapid reactions of platelets studied by a quenched-flow approach: aggregation kinetics. J Lab Clin Med 100(6):866–886. doi:10.1111/j.1365-2141.1984.tb03969.x

Goldsmith HL, Turitto VT (1986) Rehological aspects of thrombosis and haemostasis: basic principles and applications. ICTH-Report-Subcommittee on Rheology of the International Committee on Thrombosis and Haemostasis. Thrombo Haemost 55(3):415–435 ISSN: 0340-6245

Goodman PD, Barlow ET, Crapo PM, Mohammad SF, Solen KA (2005) Computational model of device-induced thrombosis and thromboembolism. Ann Biomed Eng 33(6):780–797. doi:10.1007/s10439-005-2951-z

Gottschall JL, Rzad L, Aster RH (1986) Studies of the minimum temperature at which human platelets can be stored with full maintenance of viability. Transfusion 26(5):460–462. doi:10.1046/j.1537-2995.1986.26587020126.x

Guj G, Stella F (1988) Numerical solutions of high-Re recirculating flows in vorticity-velocity form. Int J Numer Methods Fluids 8(4):405–416. doi:10.1002/fld.1650080404

Hansen KB, Arzani A, Shadden SC (2015) Mechanical platelet activation in abdominal aortic aneurysms. J Biomech Eng 137:041005–1–8. doi:10.1115/1.4029580

Holme S, Heaton A (1995) In vitro platelet ageing at 22 °C is reduced compared to in vivo ageing at 37 °C. Br J Haematol 91(1):212–218. doi:10.1111/j.1365-2141.1995.tb05272.x

Holmsen H, Weiss HJ (1979) Secretable storage pools in platelets. Ann Rev Med 30:119–134. doi:10.1146/annurev.me.30.020179.001003

Hubbell JA, McIntire LV (1986a) Platelet active concentration profiles near growing thrombi. Biophys J 50:937–945. doi:10.1016/S0006-3495(86)83535-4

Hubbell JA, McIntire LV (1986b) Visualization and analysis of mural thrombogenesis on collagen, polyurethane and nylon. Biomaterials 7:354–363. doi:10.1016/0142-9612(86)90006-2

Karino T, Goldsmith HL (1979) Adhesion of human platelets to collagen on the walls distal to a tubular expansion. Microvasc Res 17:238–262. doi:10.1016/S0026-2862(79)80002-3

Kennedy SD, Igarashi Y, Kickler TS (1997) Measurement of in vitro P-selectin expression by flow cytometry. Am J Clin Pathol 107:99–104 ISSN: 0002-9173

Leiderman K, Fogelson AL (2011) Grow with the flow: a spatial-temporal model of platelet deposition and blood coagulation under flow. Math Med Biol 28:47–84. doi:10.1093/imammb/dqq005

Leiderman K, Fogelson AL (2014) An overview of mathematical modeling of thrombus formation under flow. Thromb Res 133:S12–S14. doi:10.1016/j.thromres.2014.03.005

Medvitz RM (2008) Development and validation of a computational fluid dynamics methodology for pulsatile blood pump design and prediction of thrombus potential. Ph.D. Dissertation, The Pennsylvania State University

Navitsky MA, Taylor JO, Smith AB, Slattery MJ, Deutsch S, Siedlecki CA, Manning KB (2014) Platelet adhesion to polyurethane urea under pulsatile flow conditions. Artif Organs 38(12):1046–1053. doi:10.1111/aor.12296

Roache PJ (1994) Perspective—a method for uniform reporting of grid refinement studies. ASME J Fluids Eng 116(3):405–413. doi:10.1115/1.2910291

Samra S (2011) Numerical implementation of a continuum platelet aggregation model. M.S. Thesis, The Pennsylvania State University

Soares JS, Sheriff J, Bluestein D (2013) A novel mathematical model of activation and sensitization of platelets subjected to dynamic stress histories. Biomech Model Mechanobiol 12:1127–1141. doi:10.1007/s10237-013-0469-0

Sohn JL (1988) Evaluation of FIDAP on some classical laminar and turbulent benchmarks. Int J Numer Methods Fluids 8(12):1469–1490. doi:10.1002/fld.1650081202

Soloviev MV, Okazaki Y, Harasaki H (1999) Whole blood platelet aggregation in humans and animals: a comparative study. J Surg Res 82(2):180–187. doi:10.1006/jsre.1998.5543

Sorensen EN, Burgreen GW, Wagner WR, Antaki JF (1999a) Computational simulation of platelet deposition and activation: I. Model development and properties. Ann Biomed Eng 27:436–438. doi:10.1114/1.200

Sorensen EN, Burgreen GW, Wagner WR, Antaki JF (1999b) Computational simulation of platelet deposition and activation: II. Results for Poiseuille flow over collagen. Ann Biomed Eng 27:449–458. doi:10.1114/1.201

Tamagawa M, Kaneda H, Hiramoto M, Nagahama S (2009) Simulation of thrombus formation in shear flows using lattice Boltzmann method. Artif Organs 33(8):604–610. doi:10.1111/j.1525-1594.2009.00782.x

Taylor JO, Witmer KP, Neuberger T, Craven BA, Meyer RS, Deutsch S, Manning KB (2014) In vitro quantification of time dependent thrombus size using magnetic resonance imaging and computational simulations of thrombus surface shear stresses. J Biomech Eng 136:071012. doi:10.1115/1.4027613

Topper SR, Navitsky MA, Medvitz RB, Paterson EG, Siedlecki CA, Slattery MJ, Deutsch S, Rosenberg G, Manning KB (2014) The use of fluid mechanics to predict regions of microscopic thrombus formation in pulsatile VADs. Cardiovasc Eng Technol 5(1):54–69. doi:10.1007/s13239-014-0174-x

Wang W, King MR (2012) Multiscale modeling of platelet adhesion and thrombus growth. Ann Biomed Eng 40(11):2345–2354. doi:10.1007/s10439-012-0558-8

Welsh JD, Stalker TJ, Voronov R, Muthard RW, Tomaiuolo M, Diamond SL, Brass LF (2014) A systems approach to hemostasis: 1. The interdependence of thrombus architecture and agonist movements in the gaps between platelets. Blood 124(11):1808–1815. doi:10.1182/blood-2014-01-550335

Williams PT, Baker AJ (1997) Numerical simulations of laminar flow over a 3D backward-facing step. Int J Numer Methods Fluids 24(11):1159–1183. doi:10.1002/(SICI)1097-0363(19970615)24:11<1159::AID-FLD534>3.0.CO;2-R

Wufsus AR, Macera NE, Neeves KB (2013) The hydraulic permeability of blood clots as a function of fibrin and platelet density. Biophys J 104(8):1812–1823. doi:10.1016/j.bpj.2013.02.055

Xu Z, Chen N, Kamocka MM, Rosen ED, Alber M (2008) A multiscale model of thrombus development. J R Soc Interface 5:705–722. doi:10.1098/rsif.2007.1202

Xu Z, Chen N, Shadden SC, Marsden JE, Kamocka MM, Rosen ED, Alber M (2009) Study of blood flow impact on growth of thrombi using a multiscale model. Soft Matter 5:769–779. doi:10.1039/B812429A

Xu Z, Lioi J, Mu J, Kamocka MM, Liu X, Chen DZ, Rosen ED, Alber M (2010) A multiscale model of venous thrombus formation with surface-mediated control of blood coagulation cascade. Biophys J 98:1723–1732. doi:10.1016/j.bpj.2009.12.4331

Xu Z, Kamocka M, Alber M, Rosen ED (2011) Computational approaches to studying thrombus development. Arterioscler Thromb Vasc Biol 31(3):500–505. doi:10.1161/ATVBAHA.110.213397